Magnetic, magneto-optical, and structural properties of URhAl from first-principles calculations

J. Kuneš and P. Novák
Institute of Physics, Czech Academy of Sciences, Cukrovarnická 10, CZ-162 53 Prague, Czech Republic

M. Diviš
Department of Electronic Structures, Charles University, Ke Karlovu 5, CZ-121 16 Prague, Czech Republic

P. M. Oppeneer
Institute of Solid State and Materials Research, P.O. Box 270016, D-01171 Dresden, Germany
(Received 10 October 2000; published 2 May 2001)

We present a first-principles investigation of the electronic properties of the intermetallic uranium compound URhAl. Two band-structure methods are employed in our study, the full-potential augmented plane-wave (FLAPW) method, in which the spin-orbit interaction was recently implemented, and the relativistic, non-full-potential, augmented-spherical-wave method. To scrutinize the relativistic implementation of the FLAPW method, we compare the spin and orbital moments on each atom, as well as the magneto-optical Kerr spectra, as calculated with both methods. The computed quantities are remarkably consistent. With the FLAPW method we further investigate the magnetocrystalline anisotropy energy, the x-ray magnetic circular dichroism at the uranium $M_{4,5}$ edge, the equilibrium lattice volume, and the bulk modulus. The magnetocrystalline anisotropy energy is computed to be huge, 34 meV per formula unit. The calculated uranium moments exhibit an Ising-like behavior—they almost vanish when the magnetization direction is forced to lie in the uranium planes. The origin of this behavior is analyzed. The calculated optical and magneto-optical spectra, and also the equilibrium lattice parameter and bulk modulus, are found to compare well to the available experimental data, which emphasizes the itinerant character of the $5f$'s in URhAl.

DOI: 10.1103/PhysRevB.63.205111 PACS number(s): 71.20.−b, 71.28.+d, 75.30.Gw, 78.20.Ls

I. INTRODUCTION

The group of ternary uranium intermetallics with composition UTX, where T is a transition metal and X a p element, has recently attracted attention (for a review, see Ref. 1). Most of the intermetallics of this composition crystallize in the hexagonal ZrNiAl structure (sometimes called the Fe_2P structure), which contains three formula units per unit cell. The ZrNiAl structure has a layered structure, consisting of planes of uranium atoms admixed with one-third of the T atoms, that are stacked consecutively along the c axis, while two adjacent uranium planes are separated from one another by a layer consisting of the remaining T atoms and the X atoms; see Fig. 1. The uranium interlayer exchange coupling is relatively weak and depends sensitively on the specific T and X elements, which gives rise to a variety of magnetic behaviors observed in the UTX compounds.[1] Some of the UTX intermetallics are ferromagnets, such as, e.g., UPtAl (Ref. 2), while others exhibit unusual antiferromagnetic structures, such as, e.g., UNiGa (Ref. 3). A metamagnetic transition from a paramagnetic state to a ferromagnetic state has been observed[4,5] in UCoAl in magnetic fields of only 0.5 T. Also URhAl, which becomes ferromagnetic at $T_C = 27$ K has received attention.[1,6–10]

One of the key questions to be addressed when discussing actinide compounds is the degree of localization of the $5f$ electrons, which may range from nearly localized to practically itinerant, depending on the specific compound.[11,12] Since the $5f$ electrons are simultaneously involved in the chemical bonding and magnetism, a broad variety of physical properties may emerge from the degree of $5f$ localization. Also URhAl has been considered in this respect. In a polarized neutron study, magnetization-density profiles were measured which supplied evidence of a high degree of anisotropic hybridization between the $5f$ and the Rh $4d$ orbitals.[8,9] A sizable induced moment of $0.28\mu_B$ on the Rh atom within the basal uranium plane was detected, whereas, interestingly, only a very small induced moment of $0.03\mu_B$ was detected on the equally close Rh site out of the plane.[8] Later inelastic neutron-scattering experiments, however, found a peak at 380 meV, which was interpreted as the signature of an intermultiplet transition,[10] promoting thus the localized picture. The 380-meV peak occurred at the same energy where a uranium intermultiplet transition was observed[13] in UPd_3, which is one of the uranium compounds where the $5f$ electrons are undoubtedly localized.

A very unusual property that was reported for URhAl is the enormous magnetocrystalline anisotropy.[1,6] The suscep-

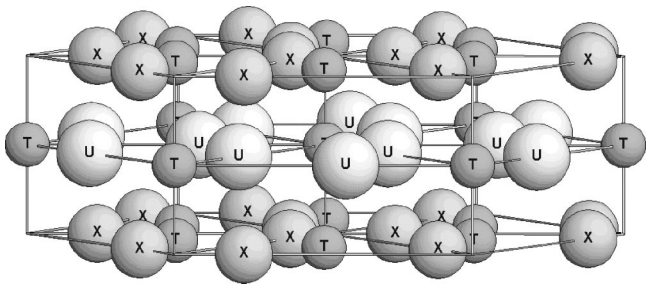

FIG. 1. The ZrNiAl-type unit cell, which is adopted by numerous UTX intermetallic compounds, with T a transition-metal element and X a p element.

tibility measured at 4.2 K for a field in the basal hexagonal plane was very different from that for a field along the *c* axis. Typically the former was identical to that of paramagnetic U compounds of the same structural group, such as, e.g., URuAl.[1] Even for fields up to 35 T only a moment of about $0.1\mu_B$ per formula unit could be induced in the basal plane. A linear extrapolation of the measured induced moments at 4.2 K would lead to an estimated field of 1500 T needed to rotate the moment into the basal plane. At elevated temperatures the magnetization can be forced to lie in the basal plane with much smaller fields. However, it was observed that the magnetization vanished when it was forced to lie in-plane.[14] The large anisotropy in the induced Rh moments that was observed in the polarized neutron study[8,9] clearly witnesses the anisotropy of the U($5f$)-Rh($4d$) hybridization: A strong hybridization occurs between the valence orbitals of the U and Rh atoms within the basal plane, but the hybridization between the valence orbitals of the U atom and those of the equally close Rh atom in the adjacent plane is much smaller.

The aim of the present study is to investigate the electronic properties of URhAl on the basis of first-principles calculations. For delocalized $5f$ electrons, the band-structure approach, based on the local-spin-density approximation (LSDA), is expected to provide an appropriate description, whereas *f*-electron materials containing localized *f* electrons tend to be better explained by specifically adapted approaches, such as, e.g., the LSDA+U approach.[15,16] Two other electronic structure calculations for URhAl were carried out recently.[15,17] These indicated, first, that the bonding and magnetism are governed by the U $5f$–Rh $4d$ hybridization,[17] and, second, that the calculated magneto-optical Kerr spectrum[15]—based on the assumption of delocalized $5f$'s—compares reasonably well to the experimental Kerr spectrum. In the present paper we address, in particular, those electronic properties which have not been explained previously. These are the magnetic moments that were measured with polarized neutrons[8,9] and with x-ray magnetic circular dichroism,[14] the enormous magnetocrystalline anisotropy energy (MAE) of approximately 41 meV per formula unit (cf. Ref. 1), the measured x-ray magnetic circular dichroism (XMCD) spectrum[14] at the uranium $M_{4,5}$ edges, and the equilibrium lattice parameter and bulk modulus.[18]

In the present electronic structure investigation we employ the full-potential linearized-augmented-plane-wave (FLAPW) method, as implemented in WIEN97 code,[19] which has recently been extended to include the relativistic spin-orbit coupling by one of us.[20] As the spin-orbit (SO) implementation is rather new, we compare our results for testing purposes to those obtained by the relativistic augmented-spherical-wave (ASW) method,[21] which is based on the spherical potential approximation. The moments as computed with both methods are remarkably consistent, as are the magneto-optical Kerr spectra.

As we will point out in detail below, the comparison of most of the calculated and experimental properties points undoubtedly to relatively delocalized $5f$ states in URhAl. One of the most interesting findings of our study is that the magnetism of URhAl is computed to be highly anisotropic. The magnetic moment of uranium, which is certainly present for magnetization along the hexagonal axis, behaves in an Ising-like manner,[22] i.e., it practically disappears when it is forced to lie perpendicular to it, in accordance with experimental observations.[14] One of the consequences is a huge computed MAE, amounting up to 34 meV per formula unit. Experimentally such an anisotropic magnetic behavior was frequently observed for UTX compounds crystalyzing in the ZrNiAl structure (cf. Ref. 1), but to our knowledge it has never been studied theoretically until now.

In the following, in Sec. II we briefly describe the implementation of SO interaction in the FLAPW scheme. We then compare the spin and orbital moments, as well as the magneto-optical Kerr effect (MOKE) spectra, as computed with the FLAPW and ASW schemes. Subsequent to the testing of the relativistic FLAPW code, in Sec. III we present our results for the equilibrium lattice parameter, the bulk modulus, the XMCD spectrum, and the MAE. Conclusions are formulated in Sec. IV.

II. COMPUTATIONAL METHOD

A. Implementation of the SO interaction

Here we briefly outline the treatment of the SO interaction in the FLAPW scheme, which is a crucial element in our study of URhAl. The FLAPW method, as implemented in the WIEN97 code,[19] was used in the present work. The standard LAPW basis with wave functions expanded into spherical harmonics inside the atomic spheres and plane waves in the interstitial space, is employed (see, e.g., Ref. 23). The starting radial basis functions inside the atomic spheres are obtained as scalar-relativistic solutions of the Dirac equation in the spherical part of the effective potential. The SO coupling is included subsequently via the second variational step approach.[24] In the first step of this approach, the scalar-relativistic part of the Hamiltonian is diagonalized on a basis adopted for each of the spin projections separately. In the second step the full Hamiltonian matrix is constructed on the basis of eigenfunctions of the first step Hamiltonian. Only a limited number of eigenstates of the first step Hamiltonian is necessary to construct the basis used in the second step. In the present implementation the size of the second step basis is controlled by an energy cutoff, so that its influence upon the results can be checked. The main approximation of this approach comes from the fact that the initial basis functions are constructed from the scalar-relativistic Hamiltonian instead of the fully relativistic Hamiltonian. This does not lead to substantial errors, because the second variational approach has been shown to yield results that are in good agreement with those of fully relativistic calculations.[25]

We neglect the SO coupling in the interstitial space. Also, for the SO coupling we consider only the spherical part of the effective potential V in the atomic spheres. The SO part of the Hamiltonian in the spheres is then given by

$$H_{so}=h_{so}(r)\,\hat{\mathbf{l}}\cdot\hat{\boldsymbol{\sigma}},\quad h_{so}(r)=\frac{\hbar}{(2Mc)^2}\frac{1}{r}\frac{dV}{dr},\qquad(1)$$

where M is the relativistically enhanced electron mass:

$$M = m + \frac{\varepsilon - V}{2c^2}. \tag{2}$$

The contribution of a given atomic sphere to the SO matrix element is given by

$$\langle i|H_{so}|j\rangle = \sum_{\substack{l,m,s,\kappa \\ m',s',\kappa'}} a^*_{lms\kappa}(i)\, a_{lm's'\kappa'}(j) \langle R^{(\kappa)}_{ls}|h_{so}|R^{(\kappa')}_{ls'}\rangle \times \langle Y_{lm}\chi_s|\hat{\mathbf{l}}\cdot\hat{\boldsymbol{\sigma}}|Y_{lm'}\chi_{s'}\rangle. \tag{3}$$

$a_{lms\kappa}(i)$ are the expansion coefficients of the function i in the spherical harmonics basis. Indices l, m, and m' correspond to the orbital quantum numbers, s and s' run over the two spin projections, and κ and κ' denote the radial function for a given expansion energy, the energy derivative of the radial function and the local orbital radial function (if used). R_{ls} is the large component of the corresponding radial function.[24] For further details, we refer to Ref. 20.

For magnetic systems the direction of the magnetization with respect to the crystal coordinate system is treated as an input parameter. It is assumed that the exchange field is unidirectional, i.e., the arrangement of the spin moments on each atomic site is collinear. The selectable magnetization direction is facilitated by rewriting the scalar product $\hat{\mathbf{l}}\cdot\hat{\boldsymbol{\sigma}}$ as[26]

$$\begin{aligned}\hat{\mathbf{l}}\cdot\hat{\boldsymbol{\sigma}} = \hat{\sigma}_z\left(\hat{l}_z\cos\theta + \frac{1}{2}\hat{l}_+ e^{-i\phi}\sin\theta + \frac{1}{2}\hat{l}_- e^{i\phi}\sin\theta\right) \\ + \frac{1}{2}\hat{\sigma}_+\left(-\hat{l}_z\sin\theta - \hat{l}_+ e^{-i\phi}\sin^2\frac{\theta}{2} + \hat{l}_- e^{i\phi}\cos^2\frac{\theta}{2}\right) \\ + \frac{1}{2}\hat{\sigma}_-\left(-\hat{l}_z\sin\theta - \hat{l}_+ e^{-i\phi}\cos^2\frac{\theta}{2} + \hat{l}_- e^{i\phi}\sin^2\frac{\theta}{2}\right),\end{aligned} \tag{4}$$

where θ and ϕ are azimuthal and polar angles of the magnetization in the rectangular crystal coordinate system. This feature allows us to study the dependence of the total energy on the exchange-field direction, which is a common method to determine the easy magnetization axis and MAE.[27]

B. Symmetry considerations

In magnetic systems the spin-orbit coupling causes rotations in the coordinate and the spinor space to be no longer independent as they are for the scalar-relativistic Hamiltonian. The symmetry is thereby reduced to at most a uniaxial one along the exchange-field direction, which may possibly increase the number of crystallographic nonequivalent atomic positions. A second consequence is that the time inversion and operations inverting the exchange field belong no longer to the symmetry group of the Hamiltonian, however, their combinations still do. This must properly be taken into account when symmetry is employed to generate eigenfunctions in the symmetry coupled k points. In the case of URhAl, whose Fe_2P crystal structure has no inversion symmetry, this aspect is of particular relevance. An immediate outcome of the symmetry considerations is that, in systems without inversion symmetry, the k-space symmetry group differs from the point group of the effective potential. This is illustrated by the example

$$R_\tau e^{i\mathbf{k}\cdot\mathbf{r}}\phi_{\mathbf{k}}(\mathbf{r}) = e^{-iR\mathbf{k}\cdot\mathbf{r}}\phi^*_{\mathbf{k}}(R^{-1}\mathbf{r}) = e^{-iR\mathbf{k}\cdot\mathbf{r}}\phi_{-R\mathbf{k}}(\mathbf{r}), \tag{5}$$

where $R_\tau = R\bigcirc\tau$ is a combined operation of a space rotation R and the time inversion τ, and the spinor part is not shown for the sake of simplicity. The consequence of Eq. (5)—for systems without inversion symmetry—is that, while R belongs to the symmetry group of the charge density and the potential, it is $-R$ that belongs to the k-space symmetry group.

III. TESTS AND RESULTS

A. Numerical aspects

In all FLAPW calculations, a regular sampling of the Brillouin zone with 838 k points was used while the sets of irreducible k points were chosen according to the symmetry imposed by the crystal structure and the exchange-field direction. For the exchange field along the c axis, an irreducible part of 1/12th Brillouin zone was used, which was enlarged to the 1/4th Brillouin zone when the exchange field was along the a axis, corresponding to the reduced symmetry of the system. The LSDA exchange-correlation parameterization of Perdew-Wang (Ref. 28) was adopted. We used a total amount of about 1260 basis functions. The uranium $6s$ and $6p$ states and rhodium $4p$ and aluminum $2p$ states were treated as local orbitals. Approximately 200 functions were used as a basis for the second variational step Hamiltonian. We found that an energy cutoff, which determines the size of the second step basis, of about 1 Ry above the Fermi level and the orbital momentum cutoff $l=4$ in Eq. (3) are sufficient for a calculation of the ground-state properties in most systems.

B. Magnetic moments

To probe the SO implementation, we compute the spin and orbital moments on each atom in URhAl, and compare these to moments computed with the ASW scheme. The calculated moments on the uranium site and on the two inequivalent rhodium sites for the magnetization along the c axis, as obtained by the two methods, are shown in Table I. In the ASW calculation 288 k points in the 1/12th irreducible part of the Brillouin zone were used. The SO coupling is treated in a second variational manner in the ASW scheme. For the exchange-correlation potential the parametrization of von Barth and Hedin[29] has been applied. The *ab initio* computed moments are found to be remarkably consistent, in spite of the quite different construction of the FLAPW and ASW basis sets and the spherical-potential versus full-potential approach. The difference per computed individual moment is less than $0.044\mu_B$. The spin moments obtained by the FLAPW method are slightly less than those of the ASW method, which can be explained by different sphere radii being used. The FLAPW atomic spheres do not overlap, and there is an interstitial contribution to the spin moment of

TABLE I. The spin magnetic moments (M_s) and orbital moments (M_l) of the individual atoms in URhAl in μ_B, as calculated by the FLAPW and ASW methods. For comparison the experimental moments as obtained from neutron diffraction experiments (Ref. 8) and the XMCD spectrum (Ref. 14) are also given.

	ASW		FLAPW		Neutr. Expt.		XMCD
	M_s	M_l	M_s	M_l	M_s	M_l	M_l
U	1.238	−1.629	1.215	−1.585	1.16	−2.10	−1.63±0.14
Rh(I)	−0.032	0.014	−0.048	0.009	0.28		
Rh(II)	−0.043	−0.010	−0.074	−0.012	0.03		

$0.379\mu_B$ per unit cell, while the ASW atomic spheres fill the space entirely and the whole spin density is distributed between them. The total spin moments per formula unit obtained by the two methods differ by $0.077\mu_B$. The good agreement obtained for the moments supports the faultlessness of the SO implementation in the FLAPW code. This further illustrates that, for this relatively closed packed material, the nonspherical potential does not have a significant influence upon the moments.

A previous calculation[17] of the spin and orbital moments of URhAl yielded very different values: a $5f$ spin (orbital) moment of $0.26\mu_B$ ($-0.10\mu_B$, respectively) on uranium was obtained, and an average d spin (orbital) moment of $-0.02\mu_B$ ($-0.003\mu_B$, respectively) on Rh. These moments do not compare favorably with our calculated moments, nor with the experimental moments. It was therefore proposed in Ref. 17 that a high-moment state exists in URhAl, which has a total energy close to the low-moment state.

In Table I we also list the experimental moments as determined from neutron-diffraction experiments[8] and from the XMCD spectrum,[14] using the XMCD sum rule for the orbital moment.[30] While the two calculations are in close correspondence with one another, the same cannot be said of the two experiments, for which the orbital moments differ by $0.5\ \mu_B$. The origin of this discrepancy in the uranium orbital moment is unknown. However, it should be mentioned that the XMCD sum rule is based on an atomic model, in which a theoretical $5f$ occupation number enters by its application. From the XMCD spectrum a high ratio of the orbital and spin moment was deduced, which was put forward as evidence of fairly localized $5f$ states.[14] The neutron-diffraction experiments, on the other hand, yielded a smaller ratio, and consequently, it was concluded that there is substantial $5f$ hybridization.[8] The calculated spin moment on U compares well to that obtained from neutron scattering, but not to that which follows from the XMCD spectrum. From the macroscopic total moment[7] of $0.94\mu_B$ a spin moment of only $(0.69\pm0.14)\mu_B$ was obtained in Ref. 14, which is considerably smaller than the computed uranium spin moment. The calculated orbital moment seems, at first sight, to be close to the XMCD orbital moment, but the common experience established by LSDA calculations for actinide materials is that the LSDA underestimates the orbital moment.[12]

To correct the underestimation of the orbital moment by the LSDA, the orbital polarization (OP) correction has been proposed.[31] The additional OP term in the Kohn-Sham equation enlarges the orbital moment,[12] and we anticipate that application of the OP to URhAl would bring the computed U orbital moment in better agreement with that measured in the polarized neutron study. Future investigations with a presently being developed OP code are envisaged.

The neutron-diffraction experiments[8,9] allocated a rather large induced magnetic moment on the Rh(I), which is the Rh atom within the uranium plane (see Fig. 1). The large induced moment of $0.28\mu_B$ was considered as evidence of U $5f$–Rh $4d$ hybridization.[8] A similarly large Rh(I) moment does not follow from our calculations. Instead, both Rh atoms are computed to be only slightly polarized with a spin polarization opposite to that of the uranium (see Table I). We can not explain this difference at present. One aspect that deserves to be mentioned is that an additional negative spin moment contribution of $-0.11\mu_B$ has been observed experimentally, which was attributed to conduction electrons.[8] While apparently further studies of URhAl are desirable, our present calculations at least provide consistent values for the moments given by LSDA band-structure theory.

C. Magneto-optical Kerr effect

A second, experimentally accessible quantity that depends crucially on the SO interaction is the MOKE.[32] The magneto-optical Kerr rotation θ_K and Kerr ellipticity ε_K are related to the optical conductivity tensor $\sigma_{\alpha\beta}$ via the expression

$$\theta_K + i\epsilon_K \approx -\frac{\sigma_{xy}}{\sigma_{xx}}\left(1+\frac{4\pi i}{\omega}\sigma_{xx}\right)^{-1/2}, \tag{6}$$

which is valid for Kerr angles and Kerr ellipticities of up to a few degrees.[33] The conductivity tensor can conveniently be calculated from its linear-response theory expression:

$$\sigma_{\alpha\beta}(\omega) = \frac{ie^2}{m^2\hbar\Omega}\sum_{\substack{\epsilon_n>\epsilon_F \\ \epsilon_m<\epsilon_F}}\frac{1}{\omega_{nm}} \times\left(\frac{\Pi^{\alpha}_{mn}\Pi^{\beta}_{nm}}{\omega-\omega_{nm}+i\delta}+\frac{\Pi^{\alpha}_{nm}\Pi^{\beta}_{mn}}{\omega+\omega_{nm}+i\delta}\right). \tag{7}$$

Here Ω is the unit-cell volume, $\hbar\omega_{nm}$ is the energy difference $\epsilon_n-\epsilon_m$, and Π_{nm} is the momentum matrix element between the occupied states m and unoccupied states n. The parameter δ accounts for the spectral broadening due to finite lifetime effects. Its determination from first principles is beyond the scope of the present single-particle approach, and therefore it is treated as a phenomenological parameter. Next

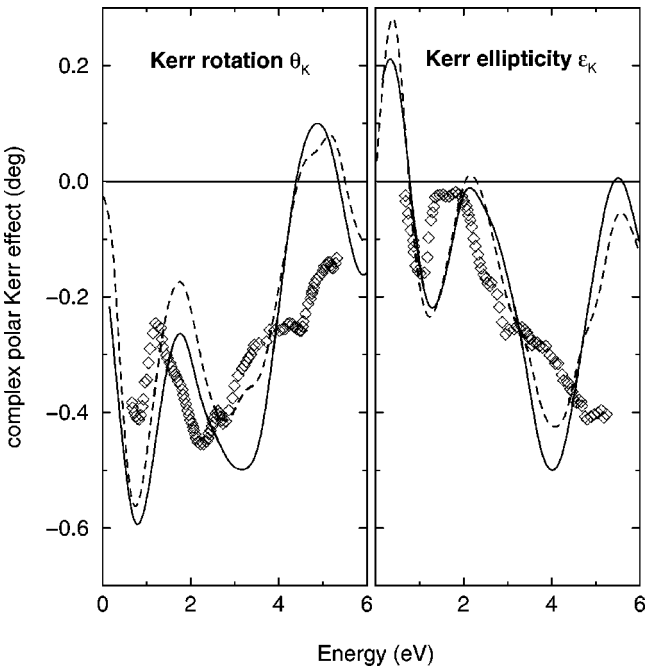

FIG. 2. The polar Kerr rotation θ_K and Kerr ellipticity ε_K for magnetization direction along the *c* axis of URhAl. The experimental data (Ref. 36) are given by the symbols, the theoretical spectra as calculated by the FLAPW scheme by the solid line, and those calculated by the ASW scheme by the dashed line.

to the optical interband conductivity spectra as given by Eq. (7), an intraband contribution of the Drude form should be added to the diagonal elements of the conductivity tensor (see, e.g., Ref. 34). For technical details of the evaluation of the conductivity tensor, we refer to Refs. 34 and 35.

The MOKE spectra, as obtained by the FLAPW and ASW methods, are compared to the experimental data[36] in Fig. 2. In the FLAPW calculation we used the same number of *k* points as in the self-consistency procedure, whereas the second-variational-step energy cutoff was increased to 2.5 Ry above the Fermi level, in order to describe better the relevant high-energy states. We checked that increasing the number of *k* points by a factor of 4, and raising the energy cutoff to 4 Ry above the Fermi level, left the spectra virtually unchanged. The intraband Drude contribution with plasma frequency $\hbar\omega_P = 3.1$ eV (calculated) was added to the diagonal elements of the conductivity tensor. Lifetime broadenings $\delta = 0.4$ and 0.6 eV were used for the interband and intraband transitions, respectively. Figure 2 shows that a good agreement between the MOKE spectra of the two different computational schemes is present over the whole energy range. Consequently, the studied SO-sensitive quantity is identically reproduced by both *ab initio* schemes. Below 4-eV photon energy, the theoretical MOKE spectra satisfactory describe both the shape and magnitude of the measured spectra. Above 4 eV there occurs a deviation of the calculated spectra from the experimental ones of Kučera *et al.*[36] The gratifying correspondence of experimental MOKE and LSDA calculations applicable for delocalized $5f$'s, suggests a relatively delocalized nature of the $5f$'s in URhAl. Optical spectra that are computed adopting localized *f* states are generally quite different from spectra computed for the same material, but assuming delocalized *f* states.[37]

D. Equilibrium volume and bulk modulus

Ground-state properties, such as the lattice parameter and bulk modulus, are generally expected to be adequately described by the LSDA density-functional formalism. Also for actinide compounds this is expected, provided the itinerant approach to the $5f$'s is warranted. We have determined the equilibrium volume and bulk modulus of URhAl by minimizing the total energy. For URhAl this is a computationally demanding task, because the unit cell contains nine atoms and there are three free internal parameters $[c/a, x(\mathrm{U}), x(\mathrm{Al})]$. In order to reduce the numerical effort, the total energies for a given unit-cell volume have been calculated at the experimental lattice parameters as obtained from pressure measurements.[18] The structural parameters $x(\mathrm{U})$ and $x(\mathrm{Al})$ have also been fixed at the experimental atomic positions, but we checked that the calculated atomic forces are quite small and thus the positions are presumably not influenced much by the volume change. The calculated total energy vs unit-cell volume has been fitted with the standard Murnaghan equation of state, from which we obtain the equilibrium volume and the bulk modulus *B*. This procedure has been carried out both for scalar-relativistic and relativistic FLAPW calculations; see Fig. 3. The scalar-relativistic FLAPW calculation yields an equilibrium volume of $V_{th}/V_{expt} = 0.957$ and a bulk modulus $B = 157$ GPa. The latter value should be compared to the experimental value $B = 175$ GPa. When SO coupling is included, the respective values are $V_{th}/V_{expt} = 0.962$ and $B = 181$ GPa (see Fig. 3), which compare favorably with the experimental values.[18] The inclusion of SO coupling obviously has a non-negligible influence on the cohesive properties. We also mention that we have found that the orbital moment decreases faster than the spin moment, with an applied pressure up to 8 GPa. The total uranium moment at 8 GPa is thereby reduced to more than 50% of the ambient pressure value. It would be of interest to test this finding experimentally.

E. Magnetocrystalline anisotropy

One of the interesting results of our study is that the magnetism of URhAl is calculated to be Ising-like, i.e., the magnetic moment practically disappears when the magnetization is forced to lie in the basal plane. A similar looking behavior exists for some rare-earth ions (e.g., Dy^{3+} in C_{3h} symmetry), where the combination of SO coupling and the axial crystal field selects, as the ground state, a Kramers doublet $|J, M_J = \pm J\rangle$, which is split when the magnetic field is along the symmetry axis, but remains nonmagnetic when the field is perpendicular to the axis.[22]

In our calculations we started from the magnetic solutions and constrained the exchange field along the *a* axis. The iterative procedure leads to a practically nonmagnetic self-consistent solution with all spin and orbital moments less than $0.02\mu_B$. The very same behavior was observed experimentally on a URhAl single crystal in an external field.[14] In order to analyze the reason for such strongly anisotropic be-

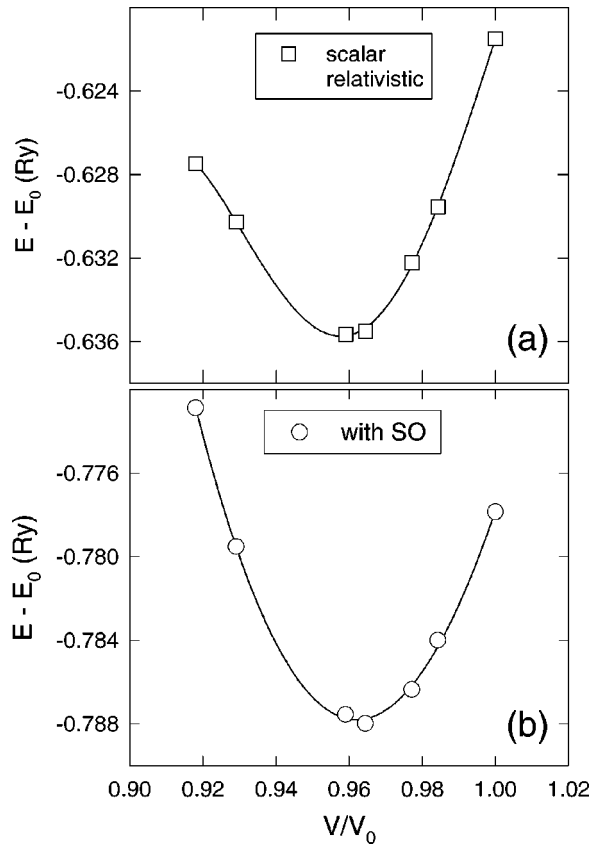

FIG. 3. The LSDA total energy of URhAl as a function of the ratio V/V_{expt}. Total energies obtained from scalar-relativistic calculations are shown in (a), and those obtained upon including the SO coupling are shown in (b). The lines are guides to the eyes.

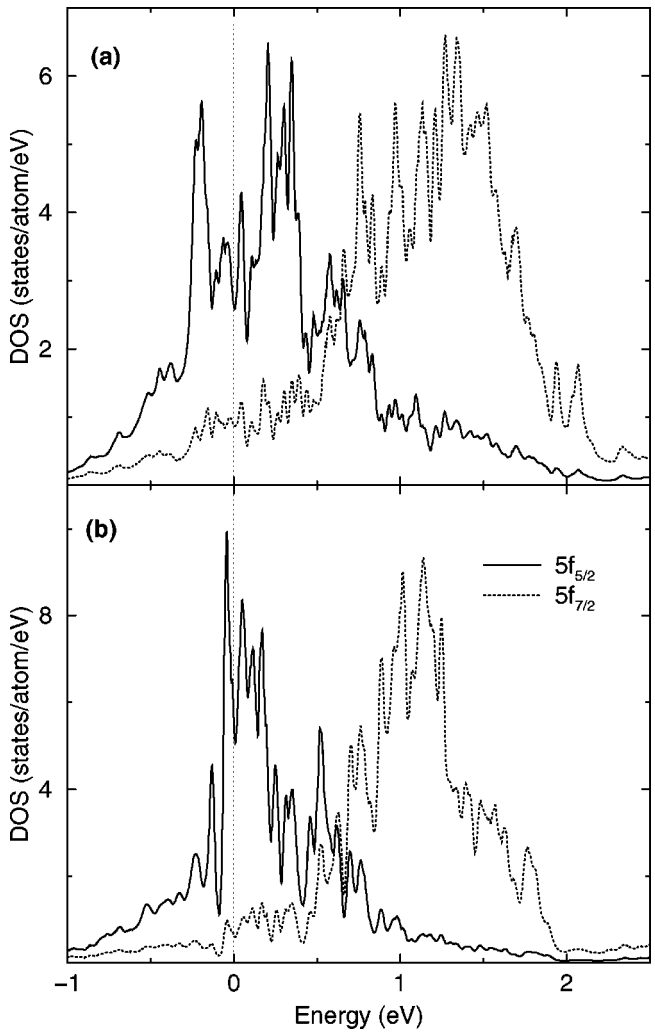

FIG. 4. The projected densities of states in the relativistic basis for *c*-axis (a) and *a*-axis (b) orientations of the exchange field. The solid line denotes the total $5f_{5/2}$ density of states and the dotted line the total $5f_{7/2}$ density of states. Note that, for both cases, the quantization axis is along the crystallographic *c* axis.

havior, we first consider the uranium site projected densities of the $5f$ states. The densities of states projected on the relativistic $j=5/2$ and 7/2 basis are shown in Fig. 4. The relativistic SO splitting of about 1 eV is clearly visible for both orientations of the exchange field. This suggests that the strength of the SO interaction is superior to that of the exchange interaction. Next we consider the densities of states projected on the $Y_{lm}\chi_s$ basis for both orientations of the exchange field, which are shown in Fig. 5. The sizes of the SO and exchange splitting can be estimated from the separation of $5f_{-3\uparrow}$ and $5f_{3\uparrow}$ states and $5f_{-3\uparrow}$ and $5f_{3\downarrow}$ states, respectively. It is apparent from Fig. 5(b) that the peak in the density of states located just below the Fermi level is formed predominantly by $5f_{-3\uparrow}$ and $5f_{3\downarrow}$ states located in the uranium planes. Their orbital counterparts $5f_{3\uparrow}$ and $5f_{-3\downarrow}$ are pushed up by the SO interaction to energies that are approximately 1 eV higher. If we now consider the stability of the nonmagnetic state in Fig. 5(b) with respect to the perturbation by an exchange field, we see readily that in a first approximation the $5f_{-3\uparrow}$ and $5f_{3\downarrow}$ states are split by the exchange field collinearly with the *c* axis, while no splitting is induced by the exchange field perpendicular to the *c* axis. In the latter case an exchange-field-induced mixing of the $5f_{-3\uparrow}$ and $5f_{3\downarrow}$ states with the $5f_{3\uparrow}$ and $5f_{-3\downarrow}$ states, or with states of different magnetic quantum numbers, is necessary for any splitting. The former possibility is prevented by the strong SO coupling. The latter would require a change in the hybridization. The fact that we obtain a nonmagnetic solution for the exchange field constrained along the *a* axis shows that exchange splitting can prevail over neither of the two above-mentioned possibilities.

Although the anisotropic ferromagnetism in URhAl looks similar to the above-mentioned Ising behavior[22] of rare-earth ions, its physical origin is different. For URhAl both the strong SO coupling and the hybridization prevent the exchange splitting for the field along the *a* axis. While the SO coupling is equally large for all U compounds, the strong hybridization is typical for the Fe_2P structure. This very anisotropic crystal structure (see Fig. 1) imposes a very anisotropic hybridization, where the U-U and U-Rh bonding in the basal plane is much stronger than the U-Rh bonding between adjacent planes. Thus the anisotropic hybridization of the $5f$'s is essential for an explanation of the unusual magnetic feature. An equivalent anisotropic magnetization behavior has, to our knowledge, never been computed for a ferromag-

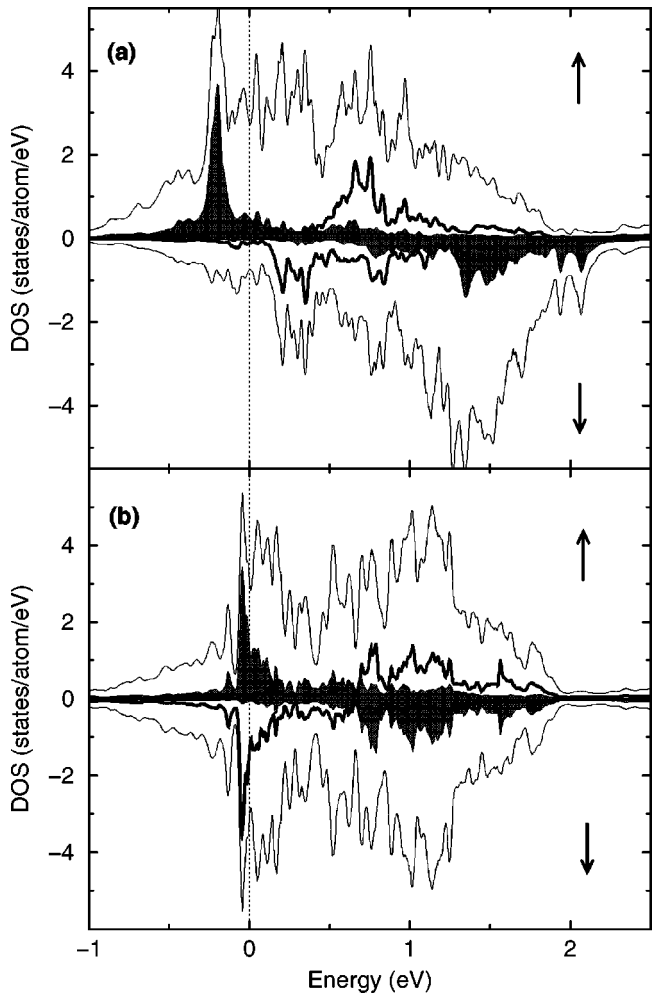

FIG. 5. Densities of states projected on the nonrelativistic $|l,m,s\rangle$ basis for *c*-axis (a) and *a*-axis (b) orientations of the exchange field. The arrows denote the spin projections. The $5f_{-3}$ states are depicted by the shaded area, the $5f_3$ states by the thick line, and the total $5f$ densities by the thin line, each for a given spin projection. The quantization axis is along the crystallographic *c*-axis.

netic material. We note, for comparison, that similar calculations[38] were performed for the layered transition-metal compounds CoPt and FePt, which belong to the magnetically hardest transition-metal materials. The spin moment in these materials was computed to be completely isotropic, whereas the orbital moment exhibited only a slight anisotropy, and a MAE of up to about 3 meV per formula unit was computed.[38] While such a value is commonly regarded as a very large MAE, for URhAl we compute an enormous MAE of 34 meV per formula unit. The strong SO coupling of uranium obviously contributes decisively to the huge MAE. An experimental value for the MAE can be obtained from the magnetization curves, which were measured for applied fields of up to 35 T along the *c* and *a* axes, respectively.[1] Assuming the magnetization curve to be linear in the applied field above 35 T, we have deduced an experimental MAE of 41 meV per formula unit. In spite of the fact that no external magnetic field is introduced in the calculation, and so the theoretically studied system is not in the experimental conditions, the computed and experimental MAE's agree fairly well with one another.

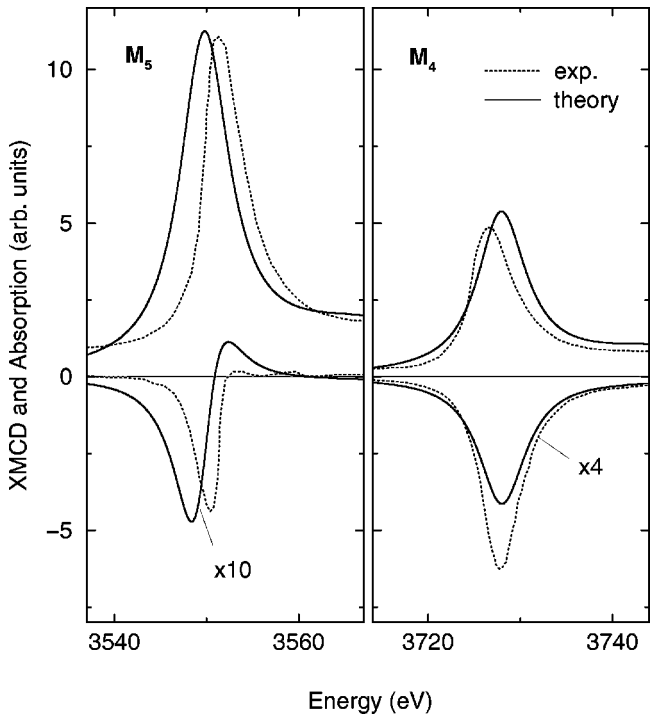

FIG. 6. Isotropic absorption spectrum (curves in the top figures) and XMCD spectrum (bottom figures) of the uranium $M_{4,5}$ edges. The *ab initio* calculated spectra are shown by the solid line, and the experimental spectra (Ref. 14) by the dotted line. Note that the XMCD spectra at the M_5 and M_4 edges have been multiplied by factors of 10 and 4, respectively.

F. X-ray magnetic circular dichroism

XMCD is a relatively new magneto-optical tool for the investigation of ferromagnetic materials. Its theoretical formulation is identical to that of the Faraday (or Kerr) effect, except that in XMCD core-valence excitations are created, whereas in the optical Faraday or Kerr effect valence-band excitations are involved. In x-ray-absorption and XMCD experiments, one measures the absorption coefficients $\alpha^{\pm}$ for the two circular polarizations of the x rays, parallel or antiparallel to the magnetization. $\alpha^{\pm}$ are related to the optical conductivity tensor:

$$\alpha^{\pm} \approx \frac{4\pi}{c} \mathrm{Re}(\sigma_{xx} \pm i\sigma_{xy}). \tag{8}$$

Due to the localized, non-dispersive character of the core states, we use different techniques for the evaluation of the optical conductivity [Eq. (7)] in the valence-band spectral range and in the x-ray spectral range.[40]

The measured and calculated x-ray absorption and XMCD spectra at the uranium $M_{4,5}$ edges are shown in Fig. 6. The $M_{4,5}$ peaks arise dominantly from transitions from the

$3d_{3/2}$ and $3d_{5/2}$ core states to the $5f$ valence states. While the splitting of the $M_{4,5}$ edges follows from the FLAPW calculation, the onset energy of the M_5 edge has been adjusted by hand. The theoretical spectra have been broadened with a Lorentzian of 3-eV width. The calculated spectra qualitatively reproduce the experimental ones. However, several differences can be observed. While the ratios of the $M_{4,5}$ absorption peaks are very similar, the experimental peaks deviate from the Lorentzian shape, which is likely caused by an energy dependence of the quasiparticle lifetime, which is not taken into account in the calculation. The major discrepancy between the calculation and experiment is the size of the M_4 XMCD peak. To quantify this discrepancy we calculated the difference between theoretical and experimental integrated XMCD peaks. For the M_4 edge this difference is 18% of the experimental XMCD spectra integrated over both edges, while in the case of the M_5 edge it is only 8%. As the integrated XMCD signal is proportional to the orbital moment[30] this discrepancy could be related to an underestimation of the orbital moment by LSDA-based computational methods. This would imply that the orbital moment obtained using the XMCD sum rule is underestimated. In order to confirm this we applied the XMCD sum rule to the theoretical spectra using the calculated $5f$ occupation of 2.5. While the calculated uranium orbital moment is $-1.59\mu_B$, the XMCD sum rule yields an orbital moment of $-1.36\mu_B$. This discrepancy is too large to be explained by a variation of the occupation number or the contribution of the *d* states to the orbital moment. It thus appears that an application of the sum rule to URhAl leads to an underestimation of the orbital moment.

The XMCD spectra can be understood qualitatively from the partial densities of states; see Fig. 5. The major contribution to the absorption at the M_4 edge stems from optical transitions to $5f_{3\downarrow}$ states (the $5f_{-3\uparrow}$ states are occupied), resulting in a single-peak structure of this part of the XMCD spectrum. The major contribution to the absorption at the M_5 edge stems from transitions to $5f_{3\uparrow}$ and $5f_{-3\downarrow}$ states, which are both unoccupied, resulting in two peaks of an opposite sign in the XMCD spectrum. As the separation of the peaks is smaller than the typical lifetime broadening, the peaks cancel each other to a large extent, thus leading to a much smaller signal than obtained at the M_4 edge.

IV. CONCLUSIONS

We have probed the recent implementation of the SO interaction in the FLAPW scheme by computing the moments and magneto-optical Kerr spectra of URhAl, and comparing these quantities to results obtained with the ASW scheme. The obtained agreement between the quantities computed with the two schemes can be regarded as outstanding.

Second, we have calculated several electronic properties of URhAl, in order to investigate the degree of $5f$ electron localization in URhAl. Two previous experimental investigations[8,9] suggested rather delocalized $5f$'s, but two more recent experiments[10,14] put forward evidence of a high degree of $5f$ localization. Our study exemplifies that the electronic properties of URhAl are very well explained by LSDA-based calculations, in which the $5f$'s are treated as itinerant. In particular, the magneto-optical Kerr effect, equilibrium volume, bulk modulus, MAE, and magnetocrystalline anisotropy of the uranium moment are satisfactory described. Somewhat less well explained are the XMCD spectrum and the uranium orbital moment, which might be connected to the insufficient treatment of OP within the LSDA.[12] The delocalized description furthermore reproduces the anomalous magnetic anisotropy that has been observed for URhAl (Ref. 14) and for other uranium intermetallic compounds that belong to the same structural group.[1] Connected with the anomalous magnetic Ising-like behavior is an enormous computed MAE of 34 meV/formula unit, compared to an experimental MAE of 41 meV/formula unit. These values considerably outrange all the MAE's that are known for transition-metal compounds, and are also three times larger than the MAE's that were recently computed for the cubic uranium monochalcogenides.[39] The origin of the large magnetic anisotropy rests in the strong SO interaction of uranium and the particular hybridization, which is typical of the very anisotropic crystal structure, that cannot be overcome by an exchange field along the *a* axis. To understand better the detailed relationship between the crystal structure and the anisotropic hybridization we are presently performing calculations for other isostructural U*TX* compounds.

Note added in proof. After this paper was accepted for publication, we performed new calculations of the electronic structure of various U*TX* compounds. For URhAl we found that beside the self-consistent solution for $M\|[100]$, as discussed above, a second self-consistent solution for this direction of *M* exists, which possesses a lower total energy. This solution has a spin moment which is only slightly reduced relative to the moment of the [001] orientation. The magnetocrystalline anisotropy energy remains large, with the *c*-axis being the easy axis. A full description of this finding will be addressed in a subsequent paper.

ACKNOWLEDGMENTS

The authors gratefully acknowledge discussions with A. V. Andreev and V. Sechovský. This work was supported financially by the German Sonderforschungsbereich 463, Dresden, Germany. The work done at Prague was supported by the GACR (Project No. 202/99/0184), GAUK (Project No. 145/2000) and GAAV (Project No. A1010715/1997), and partially by Grant No. LB98202 within the Project No. INFRA2 of the Ministry of Education, Youth, and Sports of the Czech Republic.

[1] V. Sechovský and L. Havela, in *Handbook of Magnetic Materials*, edited by K. H. J. Buschow (Elsevier, Amsterdam, 1998), Vol. 11, p. 1.
[2] V. Sechovský, L. Havela, P. Nozar, E. Brück, F. R. de Boer, A. A. Menovsky, K. H. J. Buschow, and A. V. Andreev, Physica B **163**, 103 (1990).
[3] V. Sechovský, L. Havela, P. Svoboda, A. V. Andreev, P. Burlet, K. Prokeš, H. Nakotte, F. R. de Boer, E. Brück, R. A. Robinson, and H. Maletta, J. Magn. Magn. Mater. **140-144**, 1379 (1995).
[4] A. V. Andreev, R. Z. Levitin, Y. F. Popov, and R. Y. Yumaguzhin, Zh. Eksp. Teor. Fiz. **27**, 1902 (1985) [Sov. Phys. Solid State **27**, 1145 (1985)].
[5] N. V. Mushnikov, T. Goto, K. Kamishima, H. Yamada, A. V. Andreev, Y. Shiokawa, A. Iwao, and V. Sechovský, Phys. Rev. B **59**, 6877 (1999).
[6] P. A. Veenhuizen, F. R. de Boer, V. Menovsky, V. Sechovský, and L. Havela, J. Phys. (Paris), Colloq. **49**, C8-485 (1988).
[7] P. A. Veenhuizen, J. C. P. Klaasse, F. R. de Boer, V. Sechovský, and L. Havela, J. Appl. Phys. **63**, 3064 (1988).
[8] J. A. Paixão, G. H. Lander, P. J. Brown, H. Nakotte, F. R. de Boer, and E. Brück, J. Phys.: Condens. Matter **4**, 829 (1992).
[9] J. A. Paixão, G. H. Lander, A. Delapalme, H. Nakotte, F. R. de Boer, and E. Brück, Europhys. Lett. **24**, 607 (1993).
[10] A. Hiess, L. Havela, K. Prokeš, R. S. Eccleston, and G. H. Lander, Physica B **230–232**, 89 (1997).
[11] E. Holland-Moritz and G. H. Lander, in *Handbook on the Physics and Chemistry of Rare Earths*, edited by K. A. Gschneidner, Jr., L. Eyring, G. H. Lander, and G. R. Choppin (North-Holland, Amsterdam, 1994), Vol. 19, p. 1.
[12] M. S. S. Brooks and B. Johansson, in *Handbook of Magnetic Materials*, edited by K. H. J. Buschow (North-Holland, Amsterdam, 1993), Vol. 7, p. 139.
[13] K. A. McEwen, U. Steigenberger, and J. L. Martinez, Physica B **186–188**, 670 (1993).
[14] W. Grange, M. Finazzi, J.-P. Kappler, A. Delobbe, G. Krill, Ph. Sainctavit, J.-P. Sanchez, A. Rogalev, and J. Goulon, J. Alloys Compd. **275–277**, 583 (1998).
[15] P. M. Oppeneer, A. Y. Perlov, V. N. Antonov, A. N. Yaresko, T. Kraft, and M. S. S. Brooks, J. Alloys Compd. **271–273**, 831 (1998).
[16] D. L. Price, B. R. Cooper, S.-P. Lim, and I. Avgin, Phys. Rev. B **61**, 9867 (2000).
[17] T. Gasche, M. S. S. Brooks, and B. Johansson, J. Phys.: Condens. Matter **7**, 9511 (1995).
[18] L. Havela, M. Diviš, V. Sechovský, A. V. Andreev, F. Honda, G. Oomi, Y. Méresse, and S. Heathman, J. Alloys Compd. (to be published).
[19] P. Blaha, K. Schwarz, and J. Luitz, *WIEN'97, A Full Potential Linearized Augmented Plane Wave Package for Calculating Crystal Properties* (Karlheinz Schwarz, Technical University Wien, Vienna, 1999), ISBN 3-9501031-0-4.
[20] P. Novák (unpublished).
[21] A. R. Williams, J. Kübler, and C. D. Gelatt, Phys. Rev. B **19**, 6094 (1979).
[22] A. Abragam and B. Bleaney, *Electron Paramagnetic Resonance of Transition Ions* (Clarendon Press, Oxford, 1970).
[23] D. J. Singh, *Planewaves, Pseudopotentials and the LAPW Method* (Kluwer Academic, Dordrecht, 1994).
[24] D. D. Koelling and B. N. Harmon, J. Phys. C **10**, 3107 (1977).
[25] A. H. MacDonald, W. E. Pickett, and D. D. Koelling, J. Phys. C **13**, 2675 (1980).
[26] X. Wang, R. Wu, D. Wang, and A. J. Freeman, Phys. Rev. B **54**, 61 (1996).
[27] A. J. Freeman and R. Wu, J. Magn. Magn. Mater. **100**, 497 (1991).
[28] J. P. Perdew and Y. Wang, Phys. Rev. B **45**, 13 244 (1992).
[29] U. von Barth and L. Hedin, J. Phys. C **5**, 1629 (1972).
[30] B. T. Thole, P. Carra, F. Sette, and G. van der Laan, Phys. Rev. Lett. **68**, 1943 (1992).
[31] M. S. S. Brooks, Physica B **130**, 6 (1985).
[32] P. M. Oppeneer, J. Sticht, T. Maurer, and J. Kübler, Z. Phys. B: Condens. Matter **88**, 309 (1992).
[33] P. M. Oppeneer, Habilitationsschrift, University of Technology Dresden, 1999.
[34] P. M. Oppeneer, T. Maurer, J. Sticht, and J. Kübler, Phys. Rev. B **45**, 10 924 (1992).
[35] J. Kuneš and P. Novák, J. Phys. Condens. Matter **11**, 6301 (1999).
[36] M. Kučera, P. Beránková, M. Matyáš, I. Tichý, and A. A. Menovsky, J. Alloys Compd. **271–273**, 467 (1998).
[37] A. Delin, P. M. Oppeneer, M. S. S. Brooks, T. Kraft, B. Johansson, and O. Eriksson, Phys. Rev. B **55**, R10 173 (1997).
[38] P. M. Oppeneer, J. Magn. Magn. Mater. **188**, 275 (1998).
[39] T. Kraft, Ph.D. thesis, University of Technology, Dresden, 1997.
[40] J. Kuneš, P. M. Oppeneer, H.-Ch. Mertins, F. Schäfers, A. Gaupp, W. Gudat, and P. Novák (unpublished).